A Coordinated Multitimescale Model Predictive Control for Output Power Smoothing in Hybrid Microgrid Incorporating Hydrogen Energy Storage

Muhammad Bakr Abdelghany ⓘ, *Member, IEEE*, Ahmed Al-Durra ⓘ, *Senior Member, IEEE*, Hatem H. Zeineldin ⓘ, *Senior Member, IEEE*, and Fei Gao ⓘ, *Fellow, IEEE*

Abstract—The intermittency of renewable energy sources (RESs) leads to the incorporation of energy storage systems into microgrids (MGs). In this article, a novel strategy based on model predictive control is proposed for the management of a wind–solar MG composed of RESs and a hydrogen energy storage system. The system is involved in the daily and regulation service markets, characterized by different timescales. The long-term operations related to the daily market are managed by a high-layer control, which schedules the hydrogen production and consumption to meet the load demand, maximizes the revenue by participating in the electricity market, and minimizes the operational costs. The short-term operations related to the real-time market are managed by a low-layer control (LLC), which corrects the deviations between the actual and forecasted conditions, by optimizing the power production according to the participation in the market and the short-term dynamics and constraints of the equipment. In addition, the LLC is in charge of smoothing the power provided to the grid. Numerical simulations demonstrate that the strategy effectively operates the MG by satisfying constraints and energy demands while minimizing device costs. Moreover, when compared to other strategies, the controller yields fewer state switches in the hydrogen devices, thus extending their lifespan. The efficacy of the control strategy is further validated through a lab-scale MG setup.

Index Terms—Hydrogen applications, operational cost analysis, optimal economic schedule, output power smoothing, re-electrification facilities.

I. INTRODUCTION

R ENEWABLE energy sources (RESs) utilization has substantially grown in recent decades. This trend is expected to persist and even intensify to minimize the release of gases that contribute to the greenhouse effect [1], [2], but the sporadic nature of RESs negatively impacts the profitability and the power quality of the energy systems that use these sources. Then, the use of RESs in the main grid necessitates the integration of energy storage systems (ESSs), such as hydrogen ESSs (HESSs), which are suitable for long storage periods due to their elevated energy density [3].

A microgrid (MG), which results from integrating RESs with storage systems, can work in two configurations: the islanded (or off-grid) and grid-connected (or on-grid) configurations. In the off-grid configuration, its objective is to maintain power balance independently, without external grid support. In contrast, in the on-grid configuration, the MG is configured to engage in markets actively to maximize profits. The high complexity of MGs leads to the design of control strategies that account for overall costs, degradation factors, and operating limitations of HESSs while guaranteeing the tracking of load demands and mitigating RES fluctuations. This research study designs a control framework based on model predictive control (MPC) [4] for the management of a wind–solar MG, where the functions of the HESS and its interconnection with the external grid are depicted through mixed logical dynamical (MLD) formulations [5]. Several control strategies can be found in the literature for the energy management of HESSs with RESs both in the islanded and connected configurations, e.g., [6], [7].

In the off-grid mode, the MG functions independently, efficiently managing power balance to meet demand, enhancing

system resilience, optimizing energy usage, and reducing associated costs [8]. Nair and Costa-Castelló [9] have developed MPC and heuristic approaches to enhance the effectiveness of the proposed controllers. In order to ensure the reliability of off-grid MGs equipped with HESSs, MPC strategies have been developed in [10] to mitigate the absence of inertia under transient conditions of voltage and frequency fluctuations. In [11], the MPC framework has been integrated for the purpose of optimizing economic performance and stability in islanded MGs that include photovoltaic (PV) as RESs. Furthermore, in [12], another MPC approach has been developed for enhancing the MG's autonomy and achieving fast transition responses. Kweon et al. [13] have developed a domain-enriched optimization algorithm for enhancing the dynamic resilience of islanded MGs. In [14], a two-layer controller of an island MG equipped with a hybrid-ESS and characterized by highly nonlinear attributes has been developed to ensure its long-term stability. Moreover, Tukkee et al. [15] have presented the optimal performance of islanded hybrid MGs based on an integrated techno-economic-environmental energy management system (EMS). However, the aforementioned strategies exclusively address the needs of islanded MGs and overlook the potential advantages offered by on-grid operations.

In the on-grid mode, the main objective is to maximize revenue from selling power. In [16], an MPC strategy has been developed for a solar MG aimed at profit maximization. Furthermore, Cavus et al. [17] have designed an optimal approach for grid-connected MGs, by combining the ε-variable and switched-MPC methods to minimize operational costs and maximize profits. Gbadega and Saha [18] have integrated the economic schedule of grid-connected MGs with ESSs based on adaptive MPC. In [19], an MPC framework using dynamic programming has been proposed to minimize the operational costs of a solar MG. An MPC framework for the following day's energy market of MGs with HESSs has been provided in [20] by accounting for economic and ecological factors. Boruah and Chandel [21] have developed a novel smart net-zero commercial grid-connected EMS paired with battery ESS (BESS) to carry out peak demand management. In [22], a grid-connected solar–wind energy system paired with BESS has been developed to meet industrial and residential loads based on the HOMER tool. However, the strategies mentioned above overlook the advantages of designing a cascaded control architecture to address any deviations that may arise during the real-time management of an MG coupled with an ESS.

Multilayer strategies have also been developed to address multiple tasks of the components in MGs. For example, in [23], a multilayer MPC strategy has been deployed for a grid-connected MG fueled by RESs. The initial layer focuses on determining the optimal economic schedule for the MG. In contrast, the subsequent layer optimizes revenue earned through markets, with a specific emphasis on enhancing the effectiveness of RESs and HESSs. Moreover, the optimization of the operation of MGs powered by RESs and characterized by uncertain and low inertia has been addressed in [24] by proposing a three-stage strategy. Furthermore, Hans et al. [25] have presented a multilayer MPC for MGs to manage RESs and exchange energy with outside entities. In order to enhance the effectiveness of energy management, a dual-layer MPC methodology for MG integrated with HESSs and PV has been suggested in [26], incorporating solar forecasting into the control strategy. A two-layer EMS for hybrid electrical vehicles has been presented in [27] to satisfy real-time load requirements. In [28], an EMS based on a novel hierarchical distributed MPC framework has been integrated to optimize the power allocation for multiple energy sources. Moreover, a multilayer EMS for smart MGs has been proposed in [29] by taking into account generation and demand-side flexibility. These studies, however, fail to incorporate the impact of transient states and minimum operational cycles of the hydrogen devices, which negatively affect their longevity and short-term dynamics.

Power fluctuations related to the intermittent nature of RESs can introduce small timescale fluctuations in the energy supply by posing challenges to grid reliability and stability. Thus, power smoothing strategies are necessary for MG management to ensure a stable energy supply and make renewable energy integration more efficient. In particular, solving the output power smoothing problem guarantees that the power injected into the grid is smoothed and fluctuations are reduced [30]. Many approaches have been introduced in recent years to address power smoothing. For example, the output power smoothing problem has been analyzed in [31] by proposing a receding horizon optimization strategy for both the wind farm and the HESS. This problem has been solved in [32] through a cooperative control based on the adaptive and predictive smoothing mechanisms. Models that account for degradation caused by power fluctuations have been introduced in [18]. Abdelghany et al. [33] have designed a single-layer MPC including the output power smoothing problem for a wind–hydrogen MG. In order to minimize battery degradation while preserving smoothing effectiveness, Abdalla et al. [34] have proposed a reliant monotonic charging/discharging controller for multiple BESSs connected in parallel. An optimal power flow management modeling and an optimization strategy for PV systems have been proposed in [35] to satisfy the overall system constraints. Furthermore, the output power smoothing of wind energy conversion systems has been developed in [36] to ensure the stability of wind turbines by applying a low-pass virtual filter. However, the papers above do not take advantage of multilayer strategies for the management of different electrical markets.

When MGs are controlled, it is common to distinguish between the primary, secondary, and tertiary controls, each with specific roles. In particular, the primary control ensures frequency and voltage stability and offers rapid responses to demand-generation fluctuations. The objective of the secondary control is to address frequency and voltage deviations resulting from the primary control. The tertiary control prioritizes economic considerations in MG operation, emphasizing cost minimization while addressing power generation and storage constraints. The goals of the tertiary control align with the control framework designed in this article and the literature mentioned above, as represented by the red block in Fig. 1. However, many studies in the literature have proposed strategies that align with the primary and secondary controls. For instance, in [37], detailed small-signal modeling has been presented for
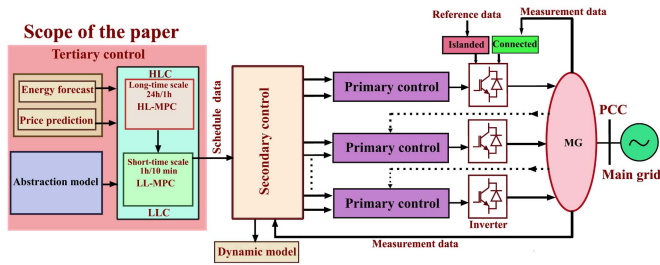
Fig. 1. Control levels of an EMS.

the primary frequency and voltage droop control. It has also shown the influence of droop gains on stability. Furthermore, in [38], an adaptive droop controller has been provided to tackle the loading effect on the primary frequency and the voltage droops and enhance the dynamic response. Aderibole et al. [39] have characterized the stability of an MG based on droop control for both inverter-based and diesel generators. In [40], an optimal control has been proposed to enhance the dynamic response of an MG and accurately track the power references without the induced control issues related to the droop. In [41], an optimization has been carried out to enhance the performance by tuning the droop controller. Regarding the secondary control, Bidram et al. [42] have developed a distributed secondary control to enhance the tracking performance of the voltage controller through feedback linearization of the nonlinearity in the controller. In [43], the stability of the secondary centralized voltage controller has been addressed, and the effects of the disturbance on the performance, such as communication delays, have been analyzed. Ahumada et al. [44] have studied the stability of the secondary centralized frequency controller on the stability of an MG. Zhang et al. [45] have enhanced the dynamic response of an MG with a distributed control by first applying input–output feedback linearization and then adding auxiliary functions for the tuning of the controller. In [46], the lead-lag compensation has been added to mitigate the delay effect on the stability of distributed secondary control in isolated MGs.

According to the authors' knowledge, none of the mentioned studies have yet proposed a multilayer MPC strategy that accounts for the output power smoothing problem, startup/shutdown and standby cycles, HESS constraints, device degradations, and operational costs for the optimal management of a HESS in a wind–solar MG operating in both the off-grid and on-grid modes. These aspects are included in the control strategy designed in this article, highlighting the innovation of the proposed approach in addressing the complex challenges of MG management. In particular, the novelties of this articles are as follows.

1) The definition of a compact model for the HESS operations based on the MLD framework that accounts for real states (on, off, and standby) and the warm start and cold start processes of the hydrogen devices (electrolyzer and fuel cell). Unlike models proposed in the literature, temporary conditions of the hydrogen devices are not included in the model as additional states, thus resulting

in a reduction of the complexity due to the number of variables.

2) The development of a unique control strategy able to manage an MG both in the off-grid and on-grid modes, thus contributing to the adaptability and resilience of the MG while optimizing its economic performance. By integrating both modes within a single framework, the need for distinct cost functions in the controller is eliminated, simplifying the control strategy and enabling smooth transitions between modes.

3) The introduction of the output power smoothing problem into a multilayer control strategy, which addresses different energy markets. This strategy finds the optimal power smoothing for the MG as the highest unconditional priority while taking into account operating constraints, logical and continuous dynamics, and degradation issues.

4) The development of a laboratory-based, real-time MG emulation to rigorously test the proposed control strategy under practical conditions.

The rest of this article is organized as follows: preliminaries and notation are given in Section II; the model of the main operations is explained in Section III; the multilayer control strategy is provided in Section IV; numerical simulations, comparisons with strategies from the literature, and experimental validations are given in Section V; finally, Section VI concludes this article.

II. PRELIMINARIES AND NOTATION

In the following, scalars are written with nonbold letters, vectors are indicated with lowercase bold letters, and matrices are written with uppercase nonbold letters. Subscripts e and f refer to the electrolyzer and the fuel cell, respectively. The device set is given by $\mathcal{D} = \{e, f\}$. The control strategies include models based on two automata. Their states are OFF, STB, and ON. Thus, the state and transition sets are $\mathcal{S} = \{\text{OFF}, \text{STB}, \text{ON}\}$ and $\mathcal{T} = \{(\alpha, \beta) \mid \alpha, \beta \in \mathcal{S}, \alpha \neq \beta\}$, with (α, β) denoting the transition from state α to state β, respectively. The logical operators AND and OR are indicated by $\wedge$ and $\vee$, respectively. Symbol $\top$ indicates the transpose, and symbol $\otimes$ denotes the Kronecker product. The n-dimensional vector space over real numbers $\mathbb{R}$ is $\mathbf{R}^n$, while $\mathbf{1}_n = (1, \ldots, 1)^\top \in \mathbf{R}^n$ and $\mathbf{0}_n = (0, \ldots, 0)^\top \in \mathbf{R}^n$ are column vectors containing n ones and zeros, respectively, and I_n denotes the $n \times n$ identity matrix. Moreover, $\mathbf{e}_i$ represents the unit column vector with value 1 in the ith position and 0 in all other positions.

This study employs a multilayer architecture, specifically distinguishing the high-layer control (HLC) and the low-layer control (LLC), whose corresponding variables are identified by superscripts h and ℓ, respectively. In cases where the distinction between the two layers is not necessary, we employ superscript n. Within the multilayer MPC framework, each optimization problem can exhibit a diverse sampling time. Particularly, we establish $\tau^h = 1$ h and $\tau^\ell = 10$ min as the designated sampling times for the HLC and the LLC, respectively. The simulation horizons employed by these two layers also differ and are labeled as T^h and T^ℓ, respectively. Moreover, variable h is used to indicate the discrete timescale for the HLC and double-variable
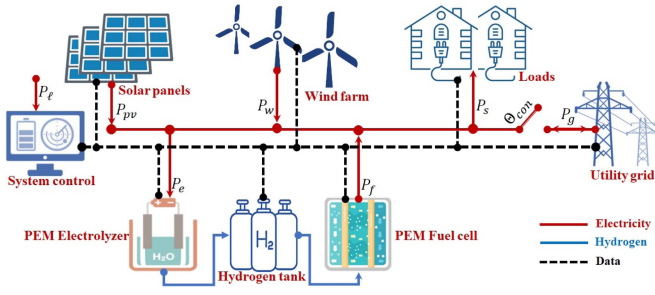
Fig. 2.   MG under investigation.

Fig. 3.   MG's interconnection with the control architecture.

(h, ℓ) to denote the timescale for the LLC, with h representing the hour (timescale of the HLC) and $\ell \in \{1, 2, \ldots, 6\}$ identifying the specific sample within that hour. When the distinction between the two controllers is not necessary, we use k and τ^n to denote the time instant and the sampling time, respectively. This practice remains consistent, even when the equations refer to distinct timescales. It is worth noting that such consistency eliminates any potential ambiguity, as the context always clarifies which timescale is applicable to the equations in question.

III. System Modeling

The system under analysis represented in Fig. 2 relies on wind and solar energies as its RESs. The main components are a wind farm, PV panels, a HESS (comprising an electrolyzer, a fuel cell, and a tank), and electrical loads. The advantages of HESS over other ESSs include efficient energy storage in the form of hydrogen gas, long-duration storage capability, scalability to meet different MG needs, and environmentally friendly operation with water vapor as the only byproduct during electricity generation. In Fig. 2, the RES powers are denoted by P_w and P_{pv}, the electrolyzer (fuel cell) power is indicated by P_e (P_f), P_l denotes the load, P_g is the power value associated with energy transactions where energy is either purchased from or sold to the utility grid, and P_s denotes the available power.

The electrical system leverages its power resources for load demand fulfillment, with any surplus energy reserved as a backup reserve. This excess energy is channeled to the electrolyzer, which, in turn, produces hydrogen that is subsequently stored in the tank. During periods of limited wind and solar energy availability, the stored hydrogen is reconverted into electricity through the use of the fuel cell and subsequently supplied to meet load requirements.

The implementation of precise control strategies is imperative to efficiently oversee the operation of these devices. The MG's interconnection with the control architecture proposed in this article is shown in Fig. 3. This architecture employs two control strategies: one for the islanded mode and another for the grid-supported mode. In the islanded mode (indicated as mod = 1), the MG operates independently, prioritizing the maintenance of power balance, system resilience, and energy efficiency. Conversely, in the grid-connected mode (denoted by mod = 2), the primary objective is to maximize revenue from power sales. These strategies operate mutually exclusively
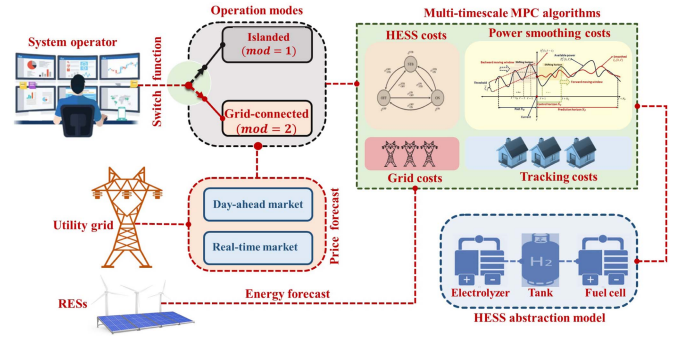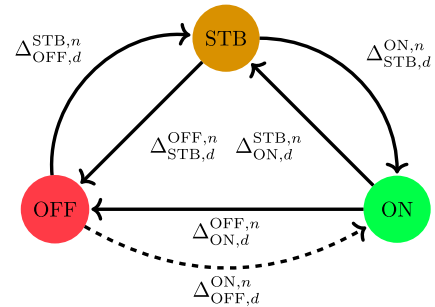

Fig. 4.   Automaton of HESS operations.

and are activated through a switching function based on the selection made by a system operator. Both strategies employ a multitimescale algorithm incorporating the HLC and the LLC for managing the system in the day-ahead and real-time markets, respectively. In particular, the HLC establishes an initial schedule on larger timescales, and then this initial schedule is adjusted by the LLC in real-time. The control strategies integrate different costs and constraints, including considerations for output power smoothing, to ensure effective system management. In particular, they aim to synchronize power injection into the grid, reduce uncertainties, and maximize profits rigorously.

A. Model of the HESS

The definition of a control framework for the operations of the MG requires, as a first step, the modeling of the system under analysis. The control strategy proposed in this article consists of two layers, namely the HLC and the LLC, which are characterized by different sampling times (and different time-steps), driven by their respective goals (day-ahead schedule for the first and real-time management for the second). However, in the MLD framework of the hydrogen devices, the same time variable k is used, even though the model will be included in both layers, which address different timescales. We will highlight the distinctions between the models used in the two layers, when relevant.

As shown in Fig. 4, the hydrogen devices are modeled by three-state automata, with state set $\mathcal{S} = \{\text{ON}, \text{STB}, \text{OFF}\}$ and transition set $\mathcal{T} = \{(\alpha, \beta) \in \mathcal{S} \times \mathcal{S} \mid \alpha \neq \beta\}$. Hence, one automaton represents the hydrogen production process (controlled
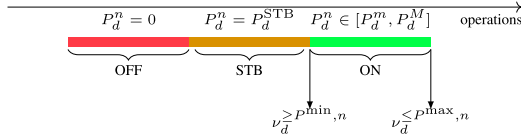
Fig. 5.   Operation power corresponding to each state.

by the electrolyzer), while another is dedicated to its consumption (managed by the fuel cell).

The nodes and the links represent the states and the switches, respectively. Particularly, ON indicates the active production (consumption) of hydrogen managed by the electrolyzer (fuel cell); OFF denotes the inactivity of the hydrogen device; STB (standby) reflects a state where the device is consuming power without being active. The inclusion of the STB state in the modeling holds significance due to the energy efficiency advantages it provides. For short periods, choosing standby over complete power-OFF reduces energy consumption during device activation. This strategy enhances the MG's efficiency, cost-effectiveness, and responsiveness to energy demand shifts. Due to the delayed response characteristics of the hydrogen devices, there is a need for a time interval in some state transitions. Specifically, a cold start process is activated for the switch transitioning from OFF to STB, while a warm start process is engaged for (STB, ON). The cold start and the warm start require some minutes, and therefore the HLC, operating on an hourly timescale, neglects them. As a consequence of these waiting processes, direct transition (OFF, ON) is not allowed and is, in fact, denoted by a dashed edge in Fig. 4.

Following the MLD framework [47], the automata are represented through the introduction of logical and continuous variables. Thus, decision variables $\Gamma_d^{\alpha,n}$ and $\Delta_{\alpha,d}^{\beta,n}$, with $n \in \{h,\ell\}$, $d \in \mathcal{D}$, and $\alpha,\beta \in \mathcal{S}$, are linked to the states and the transitions of the automata, respectively. In particular, for layer n, operation d, and state α, $\Gamma_d^{\alpha,n}$ is introduced such that it is equal to 1 if automaton d is in state α at time-step k related to layer n, and 0 otherwise. Moreover, $\Delta_{\alpha,d}^{\beta,n}$ is such that $\Delta_{\alpha,d}^{\beta,n}(k) = 1$ if the switch from α to β is enabled in automaton d at time-step k for layer n, and $\Delta_{\alpha,d}^{\beta,n}(k) = 0$ otherwise.

1) State Processes: As mentioned above, switches (STB, ON) and (OFF, STB) involve waiting processes due to the slow response of the components. Therefore, these processes are modeled through the introduction of logical variable $\Upsilon_d^{\alpha,n}$, with $n \in \{h,\ell\}$, $d \in \mathcal{D}$, and $\alpha \in \mathcal{S}$, such that $\Upsilon_d^{\alpha,n}(k) = 1$ if device d should stay in α, and $\Upsilon_d^{\alpha,n}(k) = 0$ otherwise. To provide an example, $\Upsilon_d^{\text{STB},n}(k) = 1$ and $\Gamma_d^{\text{OFF},n}(k) = 1$ indicate that operation d is OFF at the moment but should move to the STB state. However, because of the cold start, it stays in the OFF state. Conversely, $\Upsilon_d^{\text{STB},n}(k) = 1$ and $\Gamma_d^{\text{STB},n}(k) = 1$ denote that device d is in the STB state and there is no intention to change its state.

As shown in Fig. 5, decision variables $\Upsilon_d^{\alpha,n}$ are related to the power of the states. For instance, the constrain $P_d^n \in [P_d^m, P_d^M]$ must be considered to avoid any damage, where P_d^m and P_d^M are the lower and upper bounds on the operation power. In particular,

the powers related to device d are subject to the following constraints:

$$P_d^n(k) = 0 \qquad \Longleftrightarrow \qquad \Upsilon_d^{\text{OFF},n}(k) = 1 \qquad (1a)$$

$$P_d^n(k) = P_d^{\text{STB}} \qquad \Longleftrightarrow \qquad \Upsilon_d^{\text{STB},n}(k) = 1 \qquad (1b)$$

$$P_d^n(k) \in [P_d^m, P_d^M] \qquad \Longleftrightarrow \qquad \Upsilon_d^{\text{ON},n}(k) = 1 \qquad (1c)$$

which can be equivalently rewritten as mixed-integer inequalities [48] that will be incorporated in numerical solvers. In order to achieve this objective, the left-side terms in (1) are defined as linear inequalities by introducing logical variables $\nu_d^{\geq 0,n}$, $\nu_d^{\geq P^{\text{STB}},n}$, and $\nu_d^{\geq P^m,n}$, which are equal to 1 if $P_d^n \geq 0$, $P_d^n \geq P_d^{\text{STB}}$, $P_d^n \geq P_d^m$, respectively, and 0 otherwise, and $\nu_d^{\leq 0,n}$, $\nu_d^{\leq P^{\text{STB}},n}$, and $\nu_d^{\leq P^M,n}$, which are analogously defined. Thus, (1) can be rewritten as

$$M_d^n \boldsymbol{\nu}_d^{\geq,n}(k) > P_d^n(k)\mathbf{1}_3 - \mathbf{p}_d^{\geq} \qquad (2a)$$

$$M_d^n \boldsymbol{\nu}_d^{\geq,n}(k) \leq P_d^n(k)\mathbf{1}_3 - \mathbf{p}_d^{\geq} + M_d^n\mathbf{1}_3 \qquad (2b)$$

$$M_d^n \boldsymbol{\nu}_d^{\leq,n}(k) > -P_d^n(k)\mathbf{1}_3 + \mathbf{p}_d^{\leq} \qquad (2c)$$

$$M_d^n \boldsymbol{\nu}_d^{\leq,n}(k) \leq -P_d^n(k)\mathbf{1}_3 + \mathbf{p}_d^{\leq} + M_d^n\mathbf{1}_3 \qquad (2d)$$

and

$$\boldsymbol{\Upsilon}_d^n(k) \leq \boldsymbol{\nu}_d^{\geq,n}(k) \qquad (3a)$$

$$\boldsymbol{\Upsilon}_d^n(k) \leq \boldsymbol{\nu}_d^{\leq,n}(k) \qquad (3b)$$

where $M_d^n \geq \max(P_d^n - P_d^M)$, $-M_d^n \geq \max(P_d^n - P_d^m)$, $\boldsymbol{\nu}_d^{\geq,n} = (\nu_d^{\geq 0,n} \ \nu_d^{\geq P^{\text{STB}},n} \ \nu_d^{\geq P^m,n})^\top$, $\boldsymbol{\nu}_d^{\leq,n} = (\nu_d^{\leq 0,n} \ \nu_d^{\leq P^{\text{STB}},n} \ \nu_d^{\leq P^{\max},n})^\top$, $\boldsymbol{\Upsilon}_d^n = (\Upsilon_d^{\text{OFF},n} \ \Upsilon_d^{\text{STB},n} \ \Upsilon_d^{\text{ON},n})^\top$, $\mathbf{p}_d^{\geq} = (0 \ P_d^{\text{STB}} \ P_d^m)^\top$, and $\mathbf{p}_d^{\leq} = (0 \ P_d^{\text{STB}} \ P_d^M)^\top$. Furthermore, the mutually exclusive condition

$$\mathbf{1}_3^\top \boldsymbol{\Upsilon}_d^n(k) = 1 \qquad (4)$$

must be included.

2) State Transitions: The values of $\Gamma_d^{\alpha,n}$ and $\Delta_{\alpha,d}^{\beta,n}$ depend on logical variable $\Upsilon_d^{\alpha,n}$. Specifically, transitions (OFF, STB) and (STB, ON) are permitted after the completion of the cold and warm starts, respectively. These latter are defined as

$$\Delta_{\text{OFF},d}^{\text{STB},n}(k) = \Upsilon_d^{\text{STB},n}(k-\tau^c)\Upsilon_d^{\text{STB},n}(k-\tau^c+1)\cdots\Upsilon_d^{\text{STB},n}(k)$$
$$\Gamma_d^{\text{OFF},n}(k-\tau^c)\Gamma_d^{\text{OFF},n}(k-\tau^c+1)\cdots\Gamma_d^{\text{OFF},n}(k-1) \quad (5a)$$

$$\Delta_{\text{STB},d}^{\text{ON},n}(k) = \Upsilon_d^{\text{ON},n}(k-\tau^w)\Upsilon_d^{\text{ON},n}(k-\tau^w+1)\cdots\Upsilon_d^{\text{ON},n}(k)$$
$$\Gamma_d^{\text{STB},n}(k-\tau^w)\Gamma_d^{\text{STB},n}(k-\tau^w+1)\cdots\Gamma_d^{\text{STB},n}(k-1) \quad (5b)$$

where τ^c (τ^w) represents the number of time instants for the cold (warm) start. According to the first (second) definition, the transition from OFF (STB) to STB (ON) can occur only if in the last τ^c (τ^w) time instants the system was in the OFF (STB) state while concurrently expressing an intention to switch to STB (ON). By applying the MLD framework, (5a) is rewritten as

$$\Delta_{\text{OFF},d}^{\text{STB},n}(k)\mathbf{1}_{\tau^c} \leq \boldsymbol{\Upsilon}_{d,\tau^c}^{\text{STB},n}(k) \qquad (6a)$$

$$\Delta_{\text{OFF},d}^{\text{STB},n}(k)\mathbf{1}_{\tau^c} \leq \boldsymbol{\Gamma}_{d,\tau^c}^{\text{OFF},n}(k) \qquad (6b)$$

$$\Delta_{\text{OFF},d}^{\text{STB},n}(k) \geq \mathbf{1}_{\tau^c}^\top \boldsymbol{\Upsilon}_{d,\tau^c}^{\text{STB},n}(k) + \mathbf{1}_{\tau^c}^\top \boldsymbol{\Gamma}_{d,\tau^c}^{\text{OFF},n}(k) + 2\tau^c - 1 \tag{6c}$$

and (5b) is equivalent to

$$\Delta_{\text{STB},d}^{\text{ON},n}(k)\mathbf{1}_{\tau^w} \leq \boldsymbol{\Upsilon}_{d,\tau^w}^{\text{ON},n}(k) \tag{7a}$$

$$\Delta_{\text{STB},d}^{\text{ON},n}(k)\mathbf{1}_{\tau^w} \leq \boldsymbol{\Gamma}_{d,\tau^w}^{\text{STB},n}(k) \tag{7b}$$

$$\Delta_{\text{STB},d}^{\text{ON},n}(k) \geq \mathbf{1}_{\tau^w}^\top \boldsymbol{\Upsilon}_d^{\text{ON},n}(k) + \mathbf{1}_{\tau^w}^\top \boldsymbol{\Gamma}_{d,\tau^w}^{\text{STB},n}(k) + 2\tau^w - 1 \tag{7c}$$

where $\boldsymbol{\Upsilon}_{d,\tau^c}^{\text{STB},n}(k) = (\Upsilon_d^{\text{STB},n}(k-\tau^c),\dots,\Upsilon_d^{\text{STB},n}(k-1))^\top$ and $\boldsymbol{\Gamma}_{d,\tau^c}^{\text{OFF}}$, $\boldsymbol{\Upsilon}_{d,\tau^w}^{\text{ON}}$, and $\boldsymbol{\Gamma}_{d,\tau^w}^{\text{STB}}$ are similar defined. Moreover, the remaining switches are not characterized by a waiting process, and then it is

$$\Delta_{\alpha,d}^{\beta,n}(k) = \Gamma_d^{\alpha,n}(k-1)\Upsilon_d^{\beta,n}(k) \tag{8}$$

for $(\alpha,\beta) \in \{(\text{STB},\text{OFF}),(\text{ON},\text{STB}),(\text{ON},\text{OFF})\}$. The expressions in (8) are equivalent to

$$A\boldsymbol{\Delta}_d^n(k) \leq \boldsymbol{\Gamma}_d^n(k-1) \otimes \mathbf{1}_2 \tag{9a}$$

$$A\boldsymbol{\Delta}_d^n(k) \leq \boldsymbol{\Upsilon}_d^n(k) \otimes \mathbf{1}_2 \tag{9b}$$

$$A\boldsymbol{\Delta}_d^n(k) \geq \boldsymbol{\Gamma}_d^n(k-1) \otimes \mathbf{1}_2 + \boldsymbol{\Upsilon}_d^n(k) \otimes \mathbf{1}_2 - \mathbf{1}_6 \tag{9c}$$

where $A = I_3 \otimes \mathbf{1}_2^\top$ is the circular shift matrix, $\boldsymbol{\Delta}_d^n = (\Delta_{\text{OFF},d}^{\text{STB},n} \ \Delta_{\text{OFF},d}^{\text{ON}} \ \Delta_{\text{STB},d}^{\text{ON},n} \ \Delta_{\text{STB},d}^{\text{OFF},n} \ \Delta_{\text{ON},d}^{\text{OFF},n} \ \Delta_{\text{ON},d}^{\text{STB},n})^\top$, and $\boldsymbol{\Gamma}_d^n = (\Gamma_d^{\text{OFF},n} \ \Gamma_d^{\text{STB},n} \ \Gamma_d^{\text{ON},n})^\top$. It is essential to note that the cold and warm starts require some minutes to complete, and the HLC, operating on a timescale of hours, effectively ignores them. This can be obtained by setting $\tau^c = \tau^w = 0$ in (5). Thus, the definitions (5) became equivalent to (8) for all transition in the HLC. Finally, the inadmissibility of transition (OFF, ON) is described as $\Delta_{\text{OFF},d}^{\text{ON},n}(k) = 0$ for all $n \in \{h,\ell\}$, $d \in \mathcal{D}$, and time instants k. Moreover, condition

$$\mathbf{1}_6^\top \boldsymbol{\Delta}_d^n(k) \leq 1 \tag{10}$$

has to be considered for all $n \in \{h,\ell\}$ and $d \in \mathcal{D}$ since at most one switch can be enabled at each time-step.

3) State Selection: The last phase of the modeling is to define state variables Γ_d^α, which directly derives from $\Delta_{\beta,d}^{\alpha,n}$, as follows:

$$\Gamma_d^{\alpha,n}(k) = \sum_{\beta \in \mathcal{S}\setminus\{\alpha\}} \Delta_{\beta,d}^{\alpha,n}(k) + \left(1 - \sum_{(\beta,\gamma)\in\mathcal{T}} \Delta_{\beta,d}^{\gamma,n}(k)\right)\Gamma_d^{\alpha,n}(k-1). \tag{11}$$

According to this equation, the automaton is in state α at time k under the following conditions: either the state was not α at time $k-1$ and one of the switches to α is allowed at time k, or the state was already α at time-step $k-1$ and no transitions are enabled at time instant k. Moreover, the product of decision variables leads nonlinearity of the controller, and then it is necessary to define additional decision variables $\Lambda_d^{\alpha,n} = (1 - \sum_{(\beta,\gamma)\in\mathcal{T}} \Delta_{\beta,d}^{\gamma,n}(k))\Gamma_d^{\alpha,n}(k-1)$, which correspond to

$$\boldsymbol{\Lambda}_d^n(k) \leq \mathbf{1}_3 - \mathbf{1}_6 \boldsymbol{\Delta}_d^n(k)\mathbf{1}_3 \tag{12a}$$

$$\boldsymbol{\Lambda}_d^n(k) \leq \boldsymbol{\Gamma}_d^n(k-1) \tag{12b}$$

$$\boldsymbol{\Lambda}_d^n(k) \geq \boldsymbol{\Gamma}_d^n(k-1) - \mathbf{1}_6 \boldsymbol{\Delta}_d^n(k)\mathbf{1}_3 \tag{12c}$$

where $\boldsymbol{\Lambda}_d^n = (\Lambda_d^{\text{OFF},n} \ \Lambda_d^{\text{STB},n} \ \Lambda_d^{\text{ON},n})^\top$. Then, the definitions (11) in compact form become

$$\boldsymbol{\Gamma}_d^n(k) = B\boldsymbol{\Delta}_d^n(k) + \boldsymbol{\Lambda}_d^n(k) \tag{13}$$

where $B = (\mathbf{e}_2 \ \mathbf{e}_3 \ \mathbf{e}_3 \ \mathbf{e}_1 \ \mathbf{e}_1 \ \mathbf{e}_2)$ is a 3×6 suitable matrix, with $\mathbf{e}_i$ being a three-dimensional unit column vector.

B. Model of Interaction With Utility Grid

The system can operate both in the off-grid and on-grid configurations. In the latter, electricity can facilitate both the purchase and the sale of energy to and from the grid. The interconnection with the utility grid is modeled using Boolean variable Θ_g^n, which is equal to 1 if the interaction occurs, and 0 otherwise. In formula, it is

$$\Theta_g^n(k) = \begin{cases} 1, & P_g^n(k) \neq \tau_g \\ 0, & P_g^n(k) = \tau_g \end{cases} \tag{14}$$

where P_g^n represents the power value employed to determine whether the energy is purchased from (if $P_g^n(k) > \tau_g$) or sold to (if $P_g^n(k) < \tau_g$) the utility grid, $\tau_g = 0$ for the HLC, $\tau_g = (P_g^h(h))^*$ for the LLC, $(P_g^h(h))^*$ is the schedule determined by the HLC and subsequently used as a reference by the LLC to address potential discrepancies in the tracking occurring in real-time. The definitions (14) are equivalently rewritten through the definition of two logical variables Θ_b^n and Θ_s^n:

$$[\Theta_b^n(k) = 1] \iff [P_g^n(k) > \tau_g] \tag{15a}$$

$$[\Theta_s^n(k) = 1] \iff [P_g^n(k) < \tau_g]. \tag{15b}$$

The logical expressions (15) can be recast as

$$(1 \ -1)^\top P_g^n(k) - (1 \ -1)^\top \tau_g \leq M_g^n \boldsymbol{\theta}_g^n(k) \tag{16a}$$

$$(-1 \ 1)^\top P_g^n(k) + (1 \ -1)^\top \tau_g \leq M_g^n \mathbf{1}_2 - M_g^n \boldsymbol{\theta}_g^n(k) \tag{16b}$$

where $\boldsymbol{\theta}_g^n = (\Theta_b^n \ \Theta_s^n)^\top$ and M_g^n $(-M_g^n)$ is an upper bound (lower) of P_g^n. Then, auxiliary variables ν_b^n and ν_s^n represent the interconnection with the utility grid, i.e.,

$$\nu_b^n(k) = P_g^n(k)\Theta_b^n(k) \tag{17a}$$

$$\nu_s^n(k) = -P_g^n(k)\Theta_s^n(k). \tag{17b}$$

According to the MLD framework, variables ν_b^n and ν_s^n are rewritten as

$$\boldsymbol{\nu}_p^n(k) \geq -M_g^n \boldsymbol{\theta}_g^n(k) \tag{18a}$$

$$\boldsymbol{\nu}_p^n(k) \leq M_g^n \boldsymbol{\theta}_g^n(k) \tag{18b}$$

$$\boldsymbol{\nu}_p^n(k) \geq (P_g^n(k) - M_g^n)\mathbf{1}_2 + M_g^n \boldsymbol{\theta}_g^n(k) \tag{18c}$$

$$\boldsymbol{\nu}_p^n(k) \leq (P_g^n(k) - M_g^n)\mathbf{1}_2 + \boldsymbol{\theta}_g^n(k) \tag{18d}$$

where $\boldsymbol{\nu}_p^n = (\nu_b^n \ \nu_s^n)^\top$ is the vector containing the auxiliary variables.

C. Hydrogen Dynamics

The evolution of hydrogen within the tank follows:

$$H^n(k+1) = H^n(k) + \eta_e \nu_e^n(k)\tau^n - \frac{\nu_f^n(k)\tau^n}{\eta_f} \tag{19}$$

where η_e (η_f) is the efficiency of the electrolyzer (fuel cell), $\nu_e^n(k) = P_e^n(k)\Gamma_e^{\text{ON},n}(k)$ and $\nu_f^n(k) = P_f^n(k)\Gamma_f^{\text{ON},n}(k)$, with P_e^n and P_f^n being the input power of the electrolyzer and the output power of the fuel cell, respectively. The products between real and logical variables in the definitions of ν_e^n and ν_f^n lead to nonlinearities, which are managed by introducing equivalent linear inequalities, following a similar approach to that employed for (17).

D. System Constraints

The condition

$$P_{\text{re}}^n(k) + \nu_e^n(k) - \nu_f^n(k) + P_g^n(k) = P_s^n(k) \qquad (20)$$

is incorporated in the optimization problem at all time-steps k to ensure power balance. In (20), the RES power is indicated by $P_{\text{re}}^n = P_{\text{pv}}^n + P_w^n$, ν_e^n, and ν_f^n are the electrolyzer and fuel cell powers, and P_g^n and P_s^n represent the grid and system powers, respectively.

In order to ensure system stability, it is essential to maintain the power of the devices and the hydrogen level in the tank within predefined minimum and maximum thresholds, i.e.,

$$P_d^m \leq P_d^n(k) \leq P_d^M \qquad (21a)$$

$$H^m \leq H^n(k) \leq H^M \qquad (21b)$$

for $n \in \{h, \ell\}$ and $d \in \mathcal{D}$, where P_d^m, P_d^M, H^m, and H^M are the lower and upper bounds of the powers and the hydrogen level, respectively.

IV. MULTILAYER CONTROL

This study aims to integrate a cascaded control system based on MPC for the management of a wind–solar MG interfacing with the day-ahead and service regulation markets, each characterized by different timescales.

A. Control Objectives

The control strategy we propose is designed to efficiently manage the MG in Fig. 2, which can operate both in the islanded and grid-connected modes. In the islanded mode, characterized by autonomous MG operation, the controller is responsible for power balance maintenance, enhancing resilience, optimizing energy efficiency, and cost mitigation. In the grid-connected mode, the primary aim is revenue maximization through the interaction with the utility grid. In addition, the control strategy handles two different timescales associated to the primary energy markets: the day-ahead market which provides scheduling for the following day, and the real-time market which addresses short-term fluctuations, with processes occurring every $\sim$10 min. Beyond the mode management and market interactions, the controller's objectives include cost efficiency and component lifespan extension. To achieve this, the control architecture prioritizes the smoothing of the solar and wind power delivery. This enables a more effective reduction of rapid power variations, contributing to the grid's stability and the overall system's reliability.
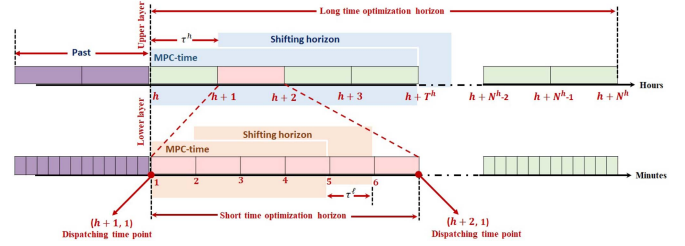

Fig. 6. Multitimescale rolling horizon optimization.

In light of the goals mentioned above, it becomes evident that the controller we develop fits with the guidelines of the tertiary control in MG management (as represented by the red block in Fig. 1). For this reason, a fundamental assumption is made: the control levels below operation management, i.e., the primary and secondary controls, are designed to maintain voltages and frequencies within desired safe operating ranges. Moreover, it is important to highlight that the fast response time and dynamic operation of the HESS contribute to the overall grid stability and reliability of the system, although on a different timescale compared to the primary and secondary controls [49], [50], [51].

The control framework adopts the MPC strategy [47], wherein the objective is to minimize the cost function at each time instant k while determining the control sequence for $j = 0, \ldots, T^n - 1$ upcoming instants, with T^n representing the planning horizon. Subsequently, the initial control decision is implemented, and the rolling horizon is moved one step forward. More specifically, MG management employs a multilayer MPC consisting of two layers: the HLC and the LLC. These layers operate with different sampling times and time-steps, related to their respective goals (day-ahead schedule for the HLC and regulation service for the LLC). As a result, the sampling times are set to $\tau^h = 1\,\text{h}$ and $\tau^\ell = 10\,\text{min}$ for the HLC and the LLC, respectively. For the sake of clarity, it is important to highlight that the LLC is executed six times within each hour, deriving from $\tau^\ell = 10\,\text{min}$. A representation of the hierarchical MPC is reported in Fig. 6, where N^h denotes the optimization horizon for the day-ahead schedule determined by the HLC. By using two timescales, we can efficiently manage a larger number of decision/optimization variables for the current time-step up to $10\,\text{min}$ ahead, while adopting fewer variables for the day ahead, where less accuracy (and higher uncertainty) is acceptable.

B. Cost Functions

At the HLC and the LLC, the corresponding cost functions are given by the integration of different terms, e.g., the grid interconnection and device operating costs. In the following, these terms and the differences between the HLC and the LLC are presented.

1) Grid Cost Functions: The cost functions associated with selling/purchasing energy from/to the utility grid for the HLC and the LLC are defined as

$$J_g^h(h) = \left(\mathbf{c}_p^h(h)\right)^\top \boldsymbol{\nu}_p^h(h)\tau^h \qquad (22a)$$

$$J_g^\ell(h,\ell) = \left(\mathbf{c}_p^\ell(h,\ell)\right)^\top \boldsymbol{\nu}_p^\ell(h,\ell)\tau^\ell \tag{22b}$$

respectively. In (22a), $\mathbf{c}_p^h(h) = ((\mathbf{c}_b^h(h))^\top - (\mathbf{c}_s^h(h))^\top)^\top$ and $\boldsymbol{\nu}_p^h(h) = ((\boldsymbol{\nu}_b^h(h))^\top (\boldsymbol{\nu}_s^h(h))^\top)^\top$, with $\mathbf{c}_b^h(h) = (c_b^h(h), \ldots, c_b^h(h+T^h))^\top$ and $\mathbf{c}_s^h(h) = (c_s^h(h), \ldots, c_s^h(h+T^h))^\top$ are the vectors of the energy sale and purchase prices at time h over horizon T^h, respectively, and $\boldsymbol{\nu}_b^h(h) = (\nu_b^\ell(h), \ldots, \nu_b^h(h+T^h))^\top$ and $\boldsymbol{\nu}_b^h(h) = (\nu_s^h(h), \ldots, \nu_s^h(h+T^h))^\top$ are the vectors of the auxiliary variables to determine the purchase or sale of energy from or to the utility grid during market activities, respectively. Similarly, in (22b), $\mathbf{c}_p^\ell(h,\ell) = ((\mathbf{c}_b^\ell(h,\ell))^\top - (\mathbf{c}_s^\ell(h,\ell))^\top)^\top$ and $\boldsymbol{\nu}_p^\ell(h,\ell) = ((\boldsymbol{\nu}_b^\ell(h,\ell))^\top (\boldsymbol{\nu}_s^\ell(h,\ell))^\top)^\top$, with $\mathbf{c}_b^\ell(h,\ell)$, $\mathbf{c}_s^\ell(h,\ell)$, $\boldsymbol{\nu}_b^\ell(h,\ell)$, and $\boldsymbol{\nu}_b^\ell(h,\ell)$ having analogous meaning of the corresponding terms of the HLC.

2) HESS Cost Functions: The HESS cost functions stem from the operations of both the electrolyzer and the fuel cell, designed to optimize cost-effectiveness and enhance longevity. Hence, these functions are formulated through the integration of depreciation of the devices, the reduction in their life cycle, and the energy consumption, i.e.,

$$
\begin{aligned}
J_d^h(h) = {}& \left(\frac{c_d^{\text{rep}}}{\text{NH}_d} + c_d^{\text{OM}}\right)(\mathbf{1}_{T^h} \otimes e_{\text{ON}})^\top \boldsymbol{\Gamma}_d^h(h) \\
& + P_d^{\text{STB}}(\mathbf{c}_{\text{sp}}^h(h))^\top (I_{T^h} \otimes e_{\text{STB}}^\top)\boldsymbol{\Gamma}_d^h(h)\tau^h \\
& + P_d^{\text{ON}}(\mathbf{c}_{\text{sp}}^h(h))^\top (I_{T^h} \otimes e_{\text{ON}}^\top)\boldsymbol{\Gamma}_d^h(h)\tau^h \\
& + (\mathbf{1}_{T^h} \otimes \mathbf{c}_t)^\top \boldsymbol{\Delta}_d^h(h)
\end{aligned}
\tag{23a}
$$

$$
\begin{aligned}
J_d^\ell(h,\ell) = {}& \left(\frac{c_d^{\text{rep}}}{\text{NH}_d} + c_d^{\text{OM}}\right)(\mathbf{1}_{T^\ell} \otimes e_{\text{ON}})^\top \boldsymbol{\Gamma}_d^\ell(h,\ell) \\
& + P_d^{\text{STB}}(\mathbf{c}_{\text{sp}}^\ell(h,\ell))^\top (I_{T^\ell} \otimes e_{\text{STB}}^\top)\boldsymbol{\Gamma}_d^\ell(h,\ell)\tau^\ell \\
& + P_d^{\text{ON}}(\mathbf{c}_{\text{sp}}^\ell(h,\ell))^\top (I_{T^\ell} \otimes e_{\text{ON}}^\top)\boldsymbol{\Gamma}_d^h(h,\ell)\tau^\ell \\
& + (\mathbf{1}_{T^\ell} \otimes \mathbf{c}_t)^\top \boldsymbol{\Delta}_d^\ell(h,\ell) \\
& + \omega_H \|\text{loh}^\ell(h,\ell) - H^h(h)\mathbf{1}_{T^\ell}\|^2 \\
& + \omega_d \|\boldsymbol{\nu}_d^\ell(h,\ell) - \nu_d^h(h)\mathbf{1}_{T^\ell}\|^2
\end{aligned}
\tag{23b}
$$

for the HLC and the LLC, respectively, with $d \in \{e, f\}$. c_d^{OM}, c_d^{rep}, and NH_d indicate the operating and maintenance cost, the stack replacement cost, and the cycles lifespan, respectively, $\mathbf{c}_t = (c_{\text{OFF}}^{\text{STB}} \; c_{\text{OFF}}^{\text{ON}} \; c_{\text{STB}}^{\text{ON}} \; c_{\text{STB}}^{\text{OFF}} \; c_{\text{ON}}^{\text{OFF}} \; c_{\text{ON}}^{\text{STB}})^\top$ is the vector of the state transition costs, $\mathbf{c}_{\text{sp}}^h$ and $\mathbf{c}_{\text{sp}}^\ell$ are the vectors of the energy spot prices over the corresponding horizon, and e_{ON} and e_{STB} are the vectors with a single unitary entry in a position such that $e_{\text{ON}}^\top \boldsymbol{\Gamma}_d^n = \Gamma_d^{\text{ON},n}$ and $e_{\text{STB}}^\top \boldsymbol{\Gamma}_d^n = \Gamma_d^{\text{STB},n}$, respectively, with $n \in \{h, \ell\}$. Moreover, the terms $\omega_H \|\text{loh}^\ell(h,\ell) - H^h\mathbf{1}_T\|^2$ and $\omega_d \|\boldsymbol{\nu}_d^\ell(h,\ell) - \nu_d^h(h)\mathbf{1}_T\|^2$ represent the hydrogen and power references provided by the HLC, where $\text{loh}^\ell(h,\ell) = (H^\ell(h,\ell), \ldots, H^\ell(h,\ell+T^\ell))^\top$ is the vector of the level of hydrogen over horizon T^ℓ, $\boldsymbol{\nu}_d^\ell$ is the vector of $\nu_d^\ell(h,\ell) = P_d^\ell(h,\ell)\Gamma_d^{\text{ON},\ell}(h,\ell)$ over horizon T^ℓ that takes the device operating power reference only at its ON state,
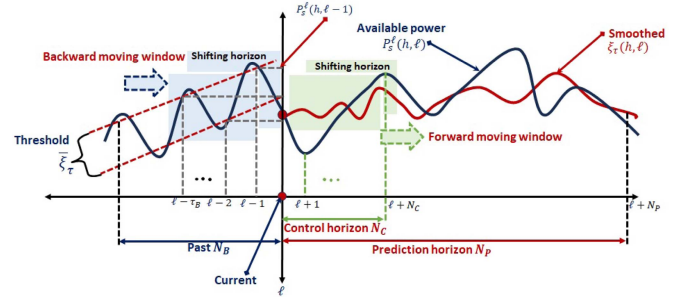

Fig. 7.   Smoothing mechanism based on consecutive previous samples of the available power.

$\nu_d^h(h) = P_d^h(h)\Gamma_d^{\text{ON},h}(h)$, and ω_H and ω_d are penalized desired weights.

3) Tracking Cost Functions: The costs related to tracking the forecasted electric reference demand are computed as

$$J_t^h(h) = \left\|\mathbf{p}_s^h(h) - \mathbf{p}_\ell(h)\right\|^2 \tag{24a}$$

$$J_t^\ell(h,\ell) = \left\|\mathbf{p}_s^\ell(h,\ell) - P_s^h(h)\mathbf{1}_{T^\ell}\right\|^2 \tag{24b}$$

for the HLC and the LLC, respectively, where $\mathbf{p}_s^h(h) = (P_s^h(h), \ldots, P_s^h(h+T^h))^\top$ and $\mathbf{p}_s^\ell(h,\ell) = (P_s^\ell(h,\ell), \ldots, P_s^\ell(h,\ell+T^\ell))^\top$ are the vectors of the available power for the HLC and the LLC, respectively, and $\mathbf{p}_\ell(h) = (P_\ell(h), \ldots, P_\ell(h+T^h))^\top$ is the vector of the load requested demand.

4) Output Power Smoothing Cost Function: The output power smoothing problem is addressed only by the LLC since its primary goal is to mitigate short-term fluctuations in the output power. This problem is achieved by accounting τ_B consecutive previous samples of the power in the system and accurately assessing future power scheduling. In particular, the controller determines an optimal output for the power in the system, denoted as P_s^ℓ, such that its variation from the previous values lies within a grid operator threshold, denoted $\bar{\xi}_\tau$. A detailed explanation of the output power smoothing mechanism is provided in Fig. 7, where the time-steps considered at current time-step ℓ in the power smoothing cost function are depicted by the blue block. The objective is to use this historical power data to establish an optimal system management strategy such that the variations in the output power for the next time-steps (in green) are bounded. This mechanism consistently maintains power variations within a fixed limit. In order to recast this problem, the corresponding cost function drives the reduction of excess delivered power slew-rate by employing a linear weight cost term structured as

$$J_{\text{avg}}^\ell(h,\ell) = \boldsymbol{\omega}_\tau(h,\ell)^\top \boldsymbol{\xi}_\tau(h,\ell) \tag{25}$$

where $\boldsymbol{\omega}_\tau(h,\ell) = (\omega_\tau(h,\ell), \ldots, \omega_\tau(h,\ell+T^\ell))^\top$ is the vector containing weights and $\boldsymbol{\xi}_\tau(h,\ell) = (\xi_\tau(h,\ell), \ldots, \xi_\tau(h,\ell+T^\ell))^\top$ is the vector of decision variables dependent on the difference between the previous and future available powers. Since the main goal is to minimize a function of the previous output powers such that the new power value remains reasonably
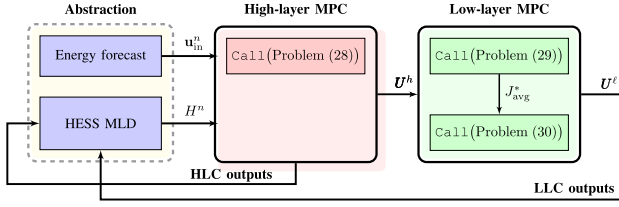
Fig. 8. Multilayer MPC control diagram.

close to them, $\boldsymbol{\xi}_\tau(h, \ell)$ is subject to the following constraints:

$$\boldsymbol{\xi}_\tau(h, \ell) \geq 0 \tag{26a}$$

$$D\boldsymbol{\xi}_\tau(h, \ell) \geq D\mathbf{p}_{\text{diff}}^\ell(h, \ell) - \bar{\xi}_\tau \mathbf{1}_{T^\ell \tau_B} \tag{26b}$$

where $\mathbf{p}_{\text{diff}}^\ell(h, \ell) = (|P_s^\ell(h, \ell) - P_s^\ell(h, \ell - \tau)|, \ldots, |P_s^\ell(h, \ell + T^\ell) - P_s^\ell(h, \ell + T^\ell - \tau)|)^\top$, $\bar{\xi}_\tau$ is the bound below which the grid operator accepts the power span, and $D = I_{T^\ell \tau_B} \otimes \mathbf{1}_{T^\ell}^\top$.

C. Optimization Problems

A schematic representation of the proposed control framework according to the multilayer MPC is given in Fig. 8. At the HLC, the forecasts of RES power P_{re}^h and electric load P_l^h for the following day are evaluated, determining the schedule for the operations of the devices and the hydrogen in the tank for the next few hours. Subsequently, the LLC corrects potential discrepancies between the actual and forecasted data using the schedule determined based on the higher layer. In Fig. 8, matrix $\boldsymbol{U}^n$ and vector $\boldsymbol{u}_{\text{in}}^n$ include the outputs and the inputs, respectively, for layer $n \in \{h, \ell\}$. In order to fulfill the goals of the islanded and grid-connected modes, the global cost function of both layers is

$$J_{\text{gs}}^n(k) = J_{\text{com}}^n(k) + \omega_g J_g^n(k)\Theta_{\text{con}}^n(k) \tag{27}$$

where $J_{\text{com}}^n(k) = \omega_e J_e^n(k) + \omega_f J_f^n(k) + \omega_t J_t^n(k)$, J_d^n, with $d \in \{e, f\}$, and J_t^n are given in (23) and (24), respectively, $J_g^n(k)$ is defined in (22), and $\omega_g, \omega_e, \omega_f$, and ω_t denote appropriate coefficients. The conditions $\Theta_{\text{con}}^n = 1$ and $\Theta_{\text{con}}^n = 0$ represent the grid-connected and standalone configurations, respectively.

The HLC manages electricity transactions for the upcoming day and fulfills the electric load. Moreover, the control objectives of the HLC depend on the current operating mode. For instance, in the on-grid configuration, the objective is to determine the most efficient schedule for the devices, ensuring effective power delivery to the grid and loads, while also minimizing the operational costs of the HESS and maximizing revenue from power sales. Conversely, the islanded mode involves effectively meeting the requested demand while prolonging the lifespan of the HESS and reducing operational and maintenance costs for the devices involved. The HLC determines as outputs reference power values for the HESS, corresponding to each hour of the day. Then, the optimization problem at the HLC is

$$\min_{\mathcal{H}_h} \quad J_{\text{gs}}^h(h)$$

s.t. Actions constraints (2)–(4)

Switches constraints (5)–(10)

Selection constraints (12)–(13)

Grid constraints (16)–(18)

Hydrogen dynamics (19)

System constraints (20)–(21) $\tag{28}$

where $\mathcal{H}_h$ is the set of decision variables at time h and J_{gs}^h is given by (27). Note that the constraints are adjusted based on discrete-time h and horizon T^h of the HLC.

The LLC must track and adjust in real-time the references obtained through optimal scheduling at the HLC. In addition, the LLC also addresses the smoothing problem. Therefore, the optimization proceeds sequentially, first minimizing the power smoothing cost function, and then employing the obtained optimal value as a constraint in the second problem aimed at minimizing the other costs. The approach ensures the highest priority on power smoothing, with the initial problem formulated as

$$(J_{\text{avg}})^* = \min_{\mathcal{L}_\ell} J_{\text{avg}}^\ell(h, \ell)$$

s.t. Similar to (28) $\tag{29}$

where J_{avg}^ℓ is defined in (25) and $\mathcal{L}_\ell$ is the set of decision variables at the LLC. The second problem is

$$\min_{\mathcal{L}_\ell} \quad J_{\text{gs}}^\ell(h, \ell)$$

s.t. Similar to (28)

Smoothing constraints (26)

$$(\boldsymbol{\omega}_\tau(h, \ell))^\top \boldsymbol{\xi}_\tau(h, \ell) \leq (J_{\text{avg}})^*. \tag{30}$$

Note that the constraints in (29) and (30) are adjusted based on discrete-time (h, ℓ) and horizon T^ℓ of the LLC.

D. Integrated Algorithm

A depiction of the integrated algorithm employing the multilayer MPC approach is presented in Algorithm 1. As previously clarified, the control algorithm integrates the optimization of multiple cost functions, encompassing load tracking, hydrogen device operations, and power smoothing.

The proposed control architecture is expressed as a mixed integer quadratic programming problem featuring multitimescale rolling optimization. An efficient solution to this problem is achieved through the branch-and-bound algorithm, with support from the commercial GUROBI solver. In this article, the control architecture is developed and analyzed in MATLAB using YALMIP/GUROBI, which allows fast execution time and efficiency. The optimization problems with simulation horizon of 24 h are resolved in 35 s at most on a PC with $Q - 4459$HQ 4.9 GHz with RAM 128 GB.

V. NUMERICAL ANALYSIS

The validation of the two-stage MPC strategy is substantiated through rigorous numerical simulations and systematic experimental analyses. Their results establish the effectiveness

Algorithm 1: Multilayer MPC Algorithm.

begin
  Load parameters;
  for $h \leftarrow 1$ **to** N^h **do**
    $\hat{\mathcal{H}}_h^{h,*} \leftarrow$ solve (28);
    $\mathcal{H}_h^* \leftarrow \hat{\mathcal{H}}_h^{h,*}\{1\}$;
    $H^h(h) \leftarrow$ update according to (19);
    for $\ell \leftarrow 1$ **to** T^ℓ **do**
      $[\hat{\mathcal{L}}_\ell^{\ell,*}, J_{\text{avg}}^*] \leftarrow$ solve (29);
      $\hat{\mathcal{L}}_\ell^{\ell,*} \leftarrow$ solve (30);
      $\mathcal{L}_\ell^* \leftarrow \hat{\mathcal{L}}_\ell^{\ell,*}\{1\}$;
      $H^\ell(h,\ell) \leftarrow$ update according to (19);
      $\ell \leftarrow \ell + 1$;
    $h \leftarrow h + 1$;

TABLE I
TECHNICAL CHARACTERISTICS OF THE DEVICES AND WEIGHTING FACTORS IN THE MULTILAYER MPC

Variable	Parameter	Value
Electrolyzer/Fuel cell parameters		
$P_e^{\min}/P_f^{\min}$	Minimum power of electrolyzer/fuel cell	0.1 MW/0.002 MW
$P_e^{\max}/P_f^{\max}$	Maximum power of electrolyzer/fuel cell	1 MW/0.1 MW
$P_e^{\text{STB}}/P_f^{\text{STB}}$	Standby consumption of electrolyzer/fuel cell	0.003 MW/0.001 MW
η_e/η_f	Efficiency of electrolyzer/fuel cell	0.015 kg/kWh/22 kWh/kg
d_e/d_f	Efficiency degradation of electrolyzer/fuel cell	4%/year/3%/year
NH_e/NH_f	Cycles lifespan of electrolyzer/fuel cell	4000 h/3000 h
NY_e/NY_f	Operation hours of electrolyzer/fuel cell	20 000 h/15 000 h
Tank parameters		
H_0^n	Initial of hydrogen tank	0.6 p.u.
$H^{\min}$	Minimum of hydrogen tank	0.1 p.u.
$H^{\max}$	Maximum of hydrogen tank	0.95 p.u.
Controller parameters		
τ^h/τ^ℓ	Sampling time for HLC/LLC	1 h/10 min
T^h/T^ℓ	Simulation horizon for HLC/LLC	24 h/1 h
ω_g^h/ω_g^ℓ	Grid coefficient for HLC/LLC	$4 \times 10^6/16 \times 10^4$
ω_e^h/ω_e^ℓ	Electrolyzer coefficient for HLC/LLC	$1 \times 10^8/1 \times 10^{12}$
ω_f^h/ω_f^ℓ	Fuel cell coefficient for HLC/LLC	$2 \times 10^4/8 \times 10^8$
$\omega_\ell^h/\omega_\ell^\ell$	Tracking coefficient for HLC/LLC	$12 \times 10^{10}/1 \times 10^6$

of the proposed controller across various scenarios. The datasets, including RES profiles and market prices employed in the analyses, have been provided by *ADNOC*, Abu Dhabi, UAE,[1] and refer to a wind farm and solar panels situated in Abu Dhabi, UAE.

The list of the characteristics of the devices, which are defined to verify the proposed approach, is reported in Table I. The coefficients of the terms included in the global cost functions are carefully determined through extensive numerical analysis to achieve a suitable balance in meeting the objectives of the hierarchical MPC. Furthermore, the analyses are conducted on a 24 h horizon for the HLC with $\tau^h = 1$ h, whereas the LLC employs $T^\ell = 1$ h with $\tau^\ell = 10$ min. The $T^h = 24$ h horizon allows for a comprehensive evaluation of energy demand and generation patterns throughout the day, capturing potential cumulative effects. Moreover, this simulation period facilitates the evaluation of the MG stability to day-to-day fluctuations in RESs and load demand.

A. Case Studies

In order to show the advantages of the multilayer MPC, the following simulations test the HLC, the LLC (with and without
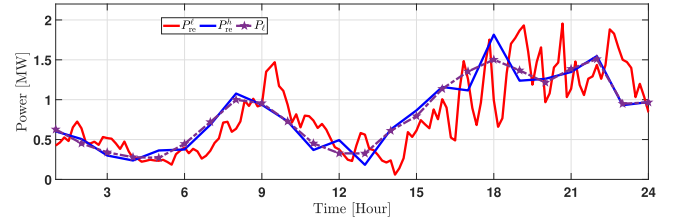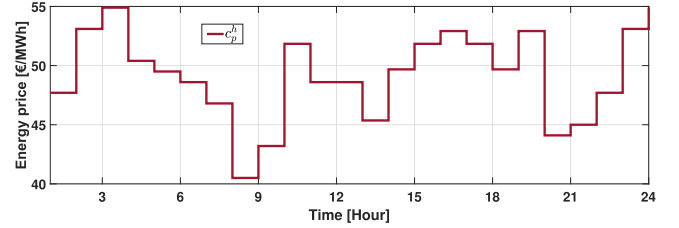
Fig. 9. RES and operator power profiles.

Fig. 10. Day-ahead market profile.

smoothing), and the integrated control strategy for both the isolated and on-grid configurations. In particular, the numerical analysis aims to show the reliability of the proposed framework in handling load demands while concurrently guaranteeing a stable and continuous power supply.

The assessment of the proposed MPC involves the evaluation of RES profiles and the corresponding electrical load illustrated in Fig. 9 for both the off-grid and on-grid modes. Fig. 10 shows the instances of electricity purchasing from and selling to the utility grid. For the sake of clarity, the energy prices are initially presented on an hourly basis and are resampled with the corresponding sampling time of 10 min at the LLC.

1) Analysis of the HLC Strategy: The HLC is required in the MG operation to manage the power exchanges for the following day and meet the requested demand (forecast). In the islanded mode (denoted by IM in the figures below), which operates without the support of the utility grid, the primary goal of the MG is to satisfy the electrical load using RESs and the hydrogen in the tank, whereas minimizing the overall costs of the devices. Conversely, in the grid-connected configuration (denoted by GC in the figures), where the MG interacts with the utility grid, it becomes crucial to consider the predicted energy prices for both energy selling and buying in the daily market. In particular, the optimization specifically aims to maximize revenue by selling power, taking into account both the available power and the day-ahead market prices. In the sequel, we assess the efficacy of the HLC under the assumption that the LLC is deactivated.

As depicted in Fig. 11, the power available in the system closely follows the load demand for both configurations over the horizon, with some exceptions occurring at hours 7, 10, and 19 in the islanded mode. Furthermore, the integrated system actively directs any surplus power generated from RESs after meeting the requested load into the electrolyzer for hydrogen production. Contrarily, in the event of a power deficit, the proposed strategy takes action by activating the fuel cell to provide extra power to
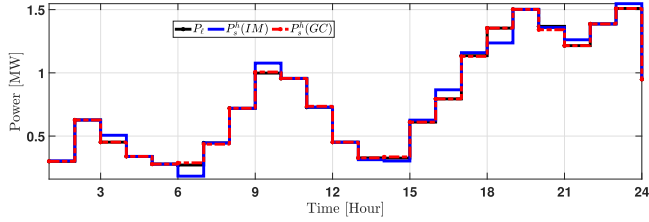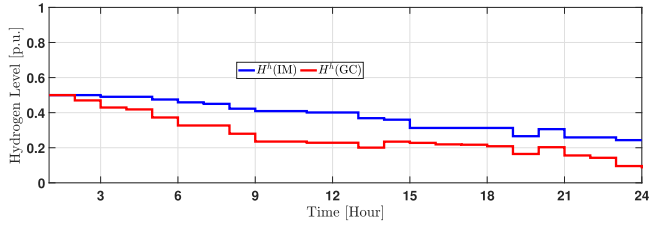
Fig. 11.   Load tracking for the HLC.
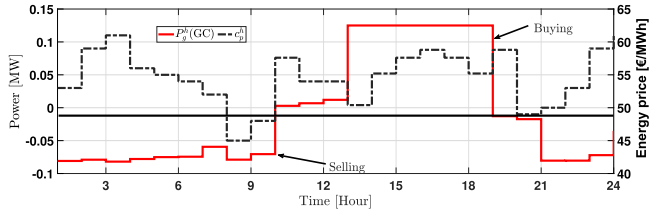

Fig. 12.   Hydrogen levels for the HLC.

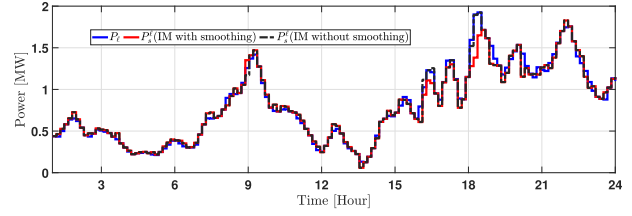Fig. 13.   Day-ahead market participation for the HLC.
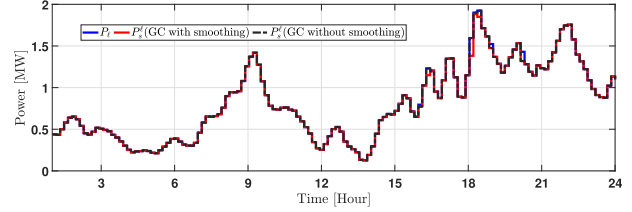

Fig. 14.   Load tracking of the LLC for the off-grid configuration.

Fig. 15.   Load tracking of the LLC for the on-grid configuration.

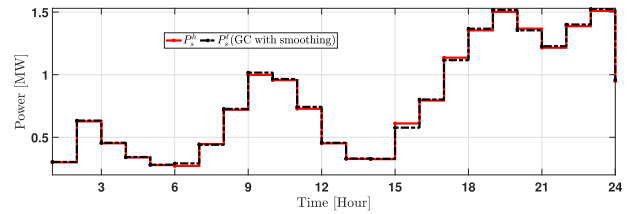Fig. 16.   Load tracking in the multilayer MPC.

the MG and guarantee the maintenance of the power balance. The corresponding levels of hydrogen are depicted in Fig. 12. In the on-grid mode, throughout the 24 h simulations excluding hours 7–9 and 19–24, the control strategy is directed toward maximizing revenues from power sold, as reported in Fig. 13.

The figures above show that the HLC effectively manages both user requests and load supply. Moreover, from the comparison between the case with and without grid support reported in Fig. 11, it becomes evident that engaging in the electricity market significantly improves the MG's ability to meet the requested load.

2) Analysis of the LLC Strategy: The main goals of the LLC are the smoothing of the RESs and the precise tracking of loads across different operational modes. To achieve this, as presented in Section IV, a multitimescale optimization is designed as follows. In the initial stage, the controller determines the optimal limits for the available power P_s^ℓ, according to the smoothing problem. These optimal bounds are subsequently used in the second optimization problem to constrain the variations of P_s^ℓ in the other costs. In the following, we demonstrate the effectiveness of the LLC under the assumption that the HLC is deactivated, and the constraint associated with the schedule derived from the HLC is neglected.

The efficacy of the proposed algorithm in managing fluctuating RES profiles is illustrated in Figs. 14 and 15 for the islanded and grid-connected configurations, respectively. The

results highlight that the system efficiently smooths the power and matches the load demand, even with fluctuating RES profiles. In Fig. 14, by comparing the application of the output power smoothing mechanism with its absence in the off-grid configuration, the differences in behavior are pronounced especially during hours 18–21, where the fluctuations in the RES profiles are more prominent. The differences, albeit to a lesser extent, are also evident in the load tracking for the on-grid configuration in Fig. 15. These reduced differences are attributed to the grid's inherent stability, enabling efficient power redistribution, and providing additional support during fluctuations. However, the results highlight the efficacy of the smoothing mechanism in ensuring reliable power delivery, particularly in the case of RES profile fluctuations.

3) Analysis of the Two-Stage MPC: One of the main goals of the multilayer MPC (given by the combination of the HLC and the LLC) is the achievement of the optimal HESS behavior despite the disagreement between the predicted scenario provided by the economic schedule from the first layer and the regulation service managed by the second layer. It is important to note that while the LLC follows the schedules defined by the HLC, it operates autonomously and can make real-time adjustments to account for deviations caused by the intermittent nature of wind and solar generation, as compared to the forecasted generation.

Figs. 16–18 show the load tracking, the hydrogen levels, and the energy market operation, respectively. It is possible to observe that the LLC follows the schedule set by the HLC by meeting the load demand. While the LLC primarily adheres to the optimal references from the HLC, it is also equipped for
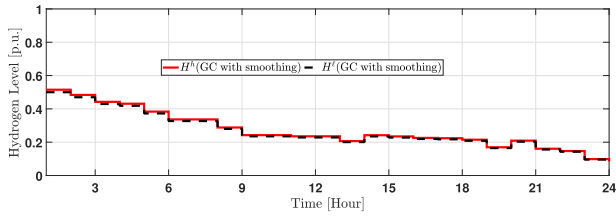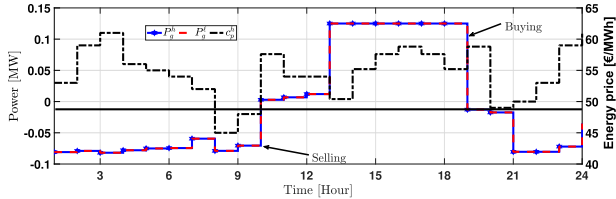
Fig. 17.   Hydrogen levels in the multilayer MPC.

Fig. 18.   Energy markets in the multilayer MPC.

Fig. 19.   Electrolyzer switches according to two-state automata-based control ([+]), five-state automata-based control ([++]), and our control (∗).

Fig. 20.   Fuel cell switches according to two-state automata-based control ([+]), five-state automata-based control ([++]), and our control (∗).

Fig. 21.   Experimental emulator setup.

autonomous system management, by ensuring adaptability in the case of deviations from the forecasted wind and solar generation. Therefore, the similarity in load tracking and hydrogen levels between the HLC and the LLC shows the effectiveness of their interconnection within the hierarchical control structure, by highlighting the coordination and the integration between the two control layers. The simulations effectively illustrate the advantages of the multilayer MPC strategy, indicating that this hierarchical control structure is a promising solution for addressing the complexities of load management and power delivery in a power system.

B. Comparison with Relevant Strategies

One of the main differences between the control strategy in this study and those from the literature lies in the model used for the hydrogen devices. The proposed model is based on three states (ON, OFF, and standby) and includes the cold start and warm start processes. On the other hand, many models in the literature, e.g., those in [18], [52], and [53], do not consider the standby state and the cold and warm starts. While these models exhibit a lower number of logical variables, they fail to capture crucial aspects such as device degradation. Moreover, other models in the literature, such as those in [54], [55], and [56], introduce two virtual states to represent the waiting actions, thus resulting in five-state automata. These models are characterized by a larger number of logical variables and inequalities: 5 state variables instead of 3, 20 transition variables instead of 6, and 115 linear inequalities instead of 40. However, the common goal of these strategies is to optimize the revenue of an MG through the electricity exchange in the energy market while simultaneously reducing the number of transitions, thus saving the equipment's lifespan.

A comparative analysis between these strategies on a 24 h simulation is shown in Figs. 19 and 20 for the electrolyzer and the fuel cell, respectively. The color denotes the states: red stands for OFF, green for ON, and yellow for STB. The comparison highlights how the control strategy based on two-state automata is required to switch the electrolyzer (fuel cell) to
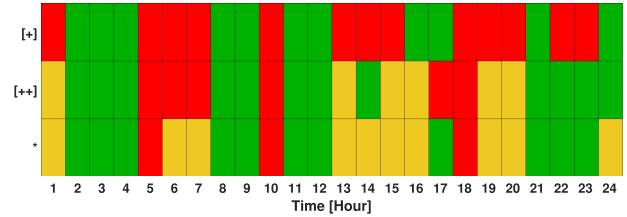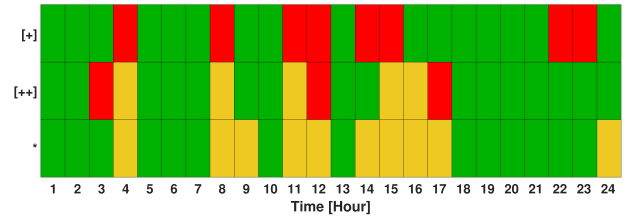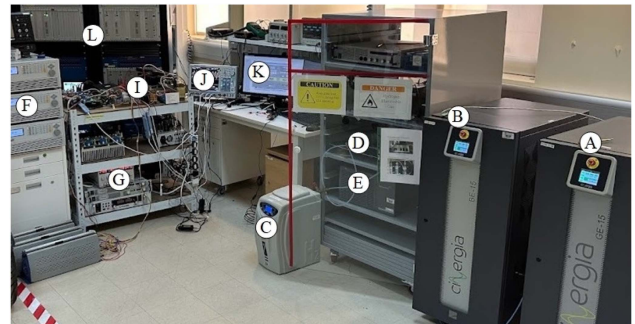
OFF even for short intervals when there is no need for hydrogen production (consumption) because of the absence of the STB state. It is important to clarify that the costs associated with transitions (OFF, STB) and (ON, STB) are lower compared to transitions (ON, OFF) and (OFF, ON). This implies that the strategy proposed in this study effectively mitigates devices' degradation and extends their operational lifespan. Moreover, the strategy based on five-state automata results in a higher number of switches compared to the proposed controller, which strategically employs the STB state. Therefore, it results that the proposed strategy effectively preserves the longevity of the hydrogen devices even when compared to complex models.

C. Experimental Validation

The proposed control framework exhibits both robustness and effectiveness using integration on a laboratory-scale MG at the *Energy Systems and Control Optimization (ESCO) Lab*, Khalifa University.[2] Fig. 21 provides a visual representation of the experimental setup designed for emulating the functioning

---

[2][Online]. Available: https://www.ku.ac.ae/facilities/energy-systems-and-control-optimization-esco-lab
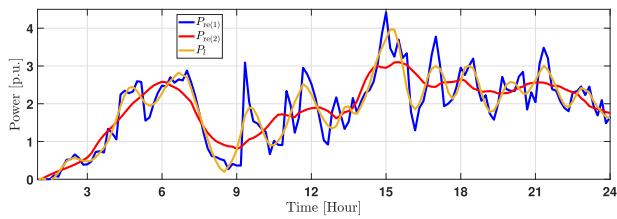
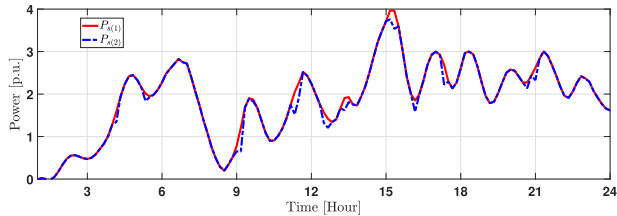Fig. 22.   Profiles used for experimental emulator setup.

Fig. 23.   Load tracking during experimental emulator setup.

of a real MG. This setup not only serves as a technical validation but also provides an understanding of the control framework's performance in practical real-world scenarios.

The simulator meticulously integrates diverse emulator components to replicate various facets of the MG. A PV emulator denoted as G, sourced from the XR160-12 family with a 20 kW capacity (*"Magna-Power"*), accurately mimics RESs. Simulating different load scenarios involves the application of an electronic load, labeled as F, with a 20 kW capacity from the Cinergia EL-15 family (*"Cinergia-EL"*). The MG setup comprises a 15 kW BESS emulator marked as B (*"Cinergia-BE"*), which is not activated in the configuration under test. Within the HESS, components such as an electrolyzer (C), a hydrogen storage tank (D), and a Nexa-1200 fuel cell (E) with a 12 kW power output (*"Nexa-FC"*) collaboratively contribute to the overall emulation. Moreover, the setup also includes a 15 kW grid emulator (A) (*"Cinergia-GE"*). The components are intricately interconnected through a power electronics interface (I), assuming an important role in controlling power flow and managing MG voltage and frequency. The comprehensive setup is complemented by an algorithm integrated into a real-time digital simulator (RTDS) indicated as L, belonging to the NovaCor family (*"NovaCor"*). This RTDS not only facilitates real-time programming of system states, but also serves as a critical element in executing the proposed algorithm. It is important to highlight that the RTDS serves as a comprehensive simulator for emulating MG components and their operations. It acts as the central processing unit, managing, and dispatching physical or simulated measures within the MG. In addition, it functions as an interface with MATLAB, which computes optimal schedules sent back to each device for their management. This interconnection is called hardware in the loop.

Fig. 22 shows the RES profiles and load demand employed for the experimental emulator setup, while Fig. 23 reports the corresponding load tracking. The results obtained from the emulator validate the efficacy of the control strategy in adeptly managing the MG configurations, thus optimizing profits and mitigating overall costs.

VI. Conclusion

This article presents a novel MPC approach for regulating MGs with a HESS. A key contribution of this work is the definition of a novel MLD model in compact form for the current operation of the HESS. The proposed MLD model is developed to be included in the MPC-based control, which addresses two conflicting objectives, namely, ensuring smooth power profiles supplied to the grid and optimizing the operation of the HESS to enhance efficiency and prolong its lifespan. The control optimization problem employs a sequential optimization technique that prioritizes power production smoothing before cost-saving operation. The efficacy of the proposed approach is shown via numerical analysis, a comparison with similar strategies from the literature, and a lab-scale setup. The results reveal that the proposed MPC enables increased lifetimes and reduced overall costs.

The controller in this study is designed to be flexible and scalable, allowing for adaptation to different sizes or capacities of the electrolyzer, the tank, the fuel cell, solar panels, and the wind farms without significant modifications. In scenarios where multiple identical components are integrated into the system, the control mechanism remains effective by either considering the total capacity and treating different units collectively or by designing specialized, low-level controllers to manage and allocate control requests to individual units. In addition, the approach can integrate different RESs alongside wind and solar powers by processing their power outputs as inputs to the controller, while adjustments are required for the inclusion of other ESSs such as batteries, leading to an increase in the number of decision variables for their management.

In the future, more advanced MPC strategies, such as distributed conditional cooperation MPC, will be used to address and incorporate the interconnected nature of different agents. Moreover, a unified architecture that integrates the proposed tertiary control with the primary and secondary control strategies will be proposed to manage both the voltage and frequency stability and economic aspects.

References

[1] C. Bernardo, L. Wang, M. Fridahl, and C. Altafini, "Quantifying leadership in climate negotiations: A social power game," *PNAS Nexus*, vol. 2, no. 11, 2023, Art. no. pgad365.

[2] A. M. Moustafa, M. B. Abdelghany, A.-S. A. Younis, M. Moness, A. Al-Durra, and J. M. Guerrero, "Software-defined control of an emulated hydrogen energy storage for energy internet ecosystems," *Int. J. Hydrogen Energy*, vol. 50, pp. 893–909, 2024.

[3] L. Valverde, F. Rosa, C. Bordons, and J. Guerra, "Energy management strategies in hydrogen smart-grids: A laboratory experience," *Int. J. Hydrogen Energy*, vol. 41, no. 31, pp. 13715–13725, 2016.

[4] A. Serna, I. Yahyaoui, J. E. Normey-Rico, C. d. Prada, and F. Tadeo, "Predictive control for hydrogen production by electrolysis in an offshore platform using renewable energies," *Int. J. Hydrogen Energy*, vol. 42, no. 17, pp. 12865–12876, 2017.

[5] C. Bernardo and F. Vasca, "A mixed logical dynamical model of the Hegselmann–Krause opinion dynamics," *IFAC-PapersOnLine*, vol. 53, no. 2, pp. 2826–2831, 2020.

[6] F. J. V. Fernández, F. S. Manzano, J. M. A. Márquez, and A. J. C. Godoy, "Extended model predictive controller to develop energy management systems in renewable source-based smart microgrids with hydrogen as backup. Theoretical foundation and case study," *Sustainability*, vol. 12, no. 21, 2020, Art. no. 8969.

[7] A. Shafiqurrahman, B. S. Umesh, N. A. Sayari, and V. Khadkikar, "Electric vehicle-to-vehicle energy transfer using on-board converters," *IEEE Trans. Transp. Electrific.*, vol. 9, no. 1, pp. 1263–1272, Mar. 2023.

[8] B. Hamad, A. Al-Durra, T. H. M. EL-Fouly, and H. H. Zeineldin, "Economically optimal and stability preserving hybrid droop control for autonomous microgrids," *IEEE Trans. Power Syst.*, vol. 38, no. 1, pp. 934–947, Jan. 2023.

[9] U. R. Nair and R. Costa-Castelló, "A model predictive control-based energy management scheme for hybrid storage system in islanded microgrids," *IEEE Access*, vol. 8, pp. 97809–97822, 2020.

[10] A. M. Taher et al., "Optimal model predictive control of energy storage devices for frequency stability of modern power systems," *J. Energy Storage*, vol. 57, 2023, Art. no. 106310.

[11] X. Zhang, C. Huang, and J. Shen, "Energy optimal management of microgrid with high photovoltaic penetration," *IEEE Trans. Ind. Appl.*, vol. 59, no. 1, pp. 128–137, Jan./Feb. 2023.

[12] J. Tobajas, F. Garcia-Torres, P. Roncero-Sánchez, J. Vázquez, L. Bellatreche, and E. Nieto, "Resilience-oriented schedule of microgrids with hybrid energy storage system using model predictive control," *Appl. Energy*, vol. 306, 2022, Art. no. 118092.

[13] J. Kweon, H. Jing, Y. Li, and V. Monga, "Small-signal stability enhancement of islanded microgrids via domain-enriched optimization," *Appl. Energy*, vol. 353, 2024, Art. no. 122172.

[14] L. Martínez, D. Fernández, and R. Mantz, "Two layer control strategy of an island DC microgrid with hydrogen storage system," *Int. J. Hydrogen Energy*, vol. 50, pp. 365–378, 2024.

[15] A. S. Tukkee, N. I. b. A. Wahab, N. F. b. Mailah, and M. K. B. Hassan, "Optimal performance of stand-alone hybrid microgrid systems based on integrated techno-economic-environmental energy management strategy using the grey wolf optimizer," *PLOS ONE*, vol. 19, no. 2, pp. 1–24, 2024.

[16] A. G. Li and M. Preindl, "Assessing degradation-aware model predictive control for energy management of a grid-connected PV-battery microgrid," in *Proc. IEEE Transp. Electrific. Conf. Expo*, 2022, pp. 546–551.

[17] M. Cavus, A. Allahham, K. Adhikari, M. Zangiabadi, and D. Giaouris, "Energy management of grid-connected microgrids using an optimal systems approach," *IEEE Access*, vol. 11, pp. 9907–9919, 2023.

[18] P. A. Gbadega and A. K. Saha, "Impact of incorporating disturbance prediction on the performance of energy management systems in micro-grid," *IEEE Access*, vol. 8, pp. 162855–162879, 2020.

[19] B. Zou et al., "Energy management of the grid-connected residential photovoltaic-battery system using model predictive control coupled with dynamic programming," *Energy Buildings*, vol. 279, 2023, Art. no. 112712.

[20] M. Daneshvar, B. Mohammadi-Ivatloo, K. Zare, and S. Asadi, "Transactive energy management for optimal scheduling of interconnected microgrids with hydrogen energy storage," *Int. J. Hydrogen Energy*, vol. 46, pp. 16267–16278, 2021.

[21] D. Boruah and S. S. Chandel, "Techno-economic feasibility analysis of a commercial grid-connected photovoltaic plant with battery energy storage-achieving a net zero energy system," *J. Energy Storage*, vol. 77, 2024, Art. no. 109984.

[22] M. R. Elkadeem et al., "Techno-enviro-socio-economic design and finite set model predictive current control of a grid-connected large-scale hybrid solar/wind energy system: A case study of Sokhna Industrial Zone, Egypt," *Energy*, vol. 289, 2024, Art. no. 129816.

[23] P. R. Mendes, L. V. Isorna, C. Bordons, and J. E. Normey-Rico, "Energy management of an experimental microgrid coupled to a V2G system," *J. Power Sources*, vol. 327, pp. 702–713, 2016.

[24] X. Qi, T. Zhao, X. Liu, and P. Wang, "Three-stage stochastic unit commitment for microgrids towards frequency security via renewable energy deloading," *IEEE Trans. Smart Grid*, vol. 14, no. 6, pp. 4256–4267, Nov. 2023.

[25] C. A. Hans, P. Braun, J. Raisch, L. Grüne, and C. Reincke-Collon, "Hierarchical distributed model predictive control of interconnected microgrids," *IEEE Trans. Sustain. Energy*, vol. 10, no. 1, pp. 407–416, Jan. 2019.

[26] H. Agharazi, M. D. Prica, and K. A. Loparo, "A two-level model predictive control-based approach for building energy management including photovoltaics, energy storage, solar forecasting, and building loads," *Energies*, vol. 15, no. 10, 2022, Art. no. 3521.

[27] P. Xie, H. Asgharian, J. M. Guerrero, J. C. Vasquez, S. S. Araya, and V. Liso, "A two-layer energy management system for a hybrid electrical passenger ship with multi-PEM fuel cell stack," *Int. J. Hydrogen Energy*, vol. 50, pp. 1005–1019, 2024.

[28] H. Liu, A. Fan, Y. Li, R. Bucknall, and L. Chen, "Hierarchical distributed MPC method for hybrid energy management: A case study of ship with variable operating conditions," *Renewable Sustain. Energy Rev.*, vol. 189, 2024, Art. no. 113894.

[29] H. Karimi and S. Jadid, "Multi-layer energy management of smart integrated-energy microgrid systems considering generation and demand-side flexibility," *Appl. Energy*, vol. 339, 2023, Art. no. 120984.

[30] L. M. S. d. Siqueira and W. Peng, "Control strategy to smooth wind power output using battery energy storage system: A review," *J. Energy Storage*, vol. 35, 2021, Art. no. 102252.

[31] E. González-Rivera, R. Sarrias-Mena, P. García-Triviño, and L. M. Fernández-Ramírez, "Predictive energy management for a wind turbine with hybrid energy storage system," *Int. J. Energy Res.*, vol. 44, no. 3, pp. 2316–2331, 2020.

[32] A. A. Abdalla, M. S. E. Moursi, T. H. M. El-Fouly, and K. H. A. Hosani, "A novel adaptive power smoothing approach for PV power plant with hybrid energy storage system," *IEEE Trans. Sustain. Energy*, vol. 14, no. 3, pp. 1457–1473, Jul. 2023.

[33] M. B. Abdelghany, M. F. Shehzad, D. Liuzza, V. Mariani, and L. Glielmo, "Modeling and optimal control of a hydrogen storage system for wind farm output power smoothing," in *Proc. IEEE 59th Conf. Decis. Control*, 2020, pp. 49–54.

[34] A. A. Abdalla, M. S. E. Moursi, T. H. M. El-Fouly, and K. H. A. Hosani, "Reliant monotonic charging controllers for parallel-connected battery storage units to reduce PV power ramp rate and battery aging," *IEEE Trans. Smart Grid*, vol. 14, no. 6, pp. 4424–4438, Nov. 2023.

[35] T. Kunatsa, H. C. Myburgh, and A. D. Freitas, "Optimal power flow management for a solar PV-powered soldier-level pico-grid," *Energies*, vol. 17, no. 2, 2024, Art. no. 459.

[36] K. Liao, D. Lu, M. Wang, and J. Yang, "A low-pass virtual filter for output power smoothing of wind energy conversion systems," *IEEE Trans. Ind. Electron.*, vol. 69, no. 12, pp. 12874–12885, Dec. 2022.

[37] N. Pogaku, M. Prodanovic, and T. C. Green, "Modeling, analysis and testing of autonomous operation of an inverter-based microgrid," *IEEE Trans. Power Electron.*, vol. 22, no. 2, pp. 613–625, Mar. 2007.

[38] Y. A.-R. I. Mohamed and E. F. El-Saadany, "Adaptive decentralized droop controller to preserve power sharing stability of paralleled inverters in distributed generation microgrids," *IEEE Trans. Power Electron.*, vol. 23, no. 6, pp. 2806–2816, Nov. 2008.

[39] A. Aderibole, H. H. Zeineldin, M. S. El-Moursi, J. C.-H. Peng, and M. A. Hosani, "Domain of stability characterization for hybrid microgrids considering different power sharing conditions," *IEEE Trans. Energy Convers.*, vol. 33, no. 1, pp. 312–323, Mar. 2018.

[40] J. F. Patarroyo-Montenegro, F. Andrade, J. M. Guerrero, and J. C. Vasquez, "A linear quadratic regulator with optimal reference tracking for three-phase inverter-based islanded microgrids," *IEEE Trans. Power Electron.*, vol. 36, no. 6, pp. 7112–7122, Jun. 2021.

[41] B. Alghamdi and C. A. Cañizares, "Frequency regulation in isolated microgrids through optimal droop gain and voltage control," *IEEE Trans. Smart Grid*, vol. 12, no. 2, pp. 988–998, Mar. 2021.

[42] A. Bidram, A. Davoudi, F. L. Lewis, and J. M. Guerrero, "Distributed cooperative secondary control of microgrids using feedback linearization," *IEEE Trans. Power Syst.*, vol. 28, no. 3, pp. 3462–3470, Aug. 2013.

[43] G. Lou, W. Gu, Y. Xu, W. Jin, and X. Du, "Stability robustness for secondary voltage control in autonomous microgrids with consideration of communication delays," *IEEE Trans. Power Syst.*, vol. 33, no. 4, pp. 4164–4178, Jul. 2018.

[44] C. Ahumada, R. Cárdenas, D. Saez, and J. M. Guerrero, "Secondary control strategies for frequency restoration in islanded microgrids with consideration of communication delays," *IEEE Trans. Smart Grid*, vol. 7, no. 3, pp. 1430–1441, May 2016.

[45] C. Zhang, X. Dou, X. Quan, Q. Hu, Z. Wu, and Y. Lv, "Distributed secondary control for island microgrids with expected dynamic performance under communication delays," *IEEE Trans. Smart Grid*, vol. 14, no. 3, pp. 2010–2022, May 2023.

[46] X. Wu et al., "Delay-dependent small-signal stability analysis and compensation method for distributed secondary control of microgrids," *IEEE Access*, vol. 7, pp. 170919–170935, 2019.

[47] A. Bemporad and M. Morari, "Control of systems integrating logic, dynamics, and constraints," *Automatica*, vol. 35, no. 3, pp. 407–427, 1999.

[48] M. B. Abdelghany and A. Al-Durra, "A coordinated model predictive control of grid-connected energy storage systems," in *Proc. Amer. Control Conf.*, 2023, pp. 1862–1867.

[49] S. D. Tavakoli et al., "Grid-forming services from hydrogen electrolyzers," *IEEE Trans. Sustain. Energy*, vol. 14, no. 4, pp. 2205–2219, Oct. 2023.

[50] M. G. Dozein, A. M. D. Corato, and P. Mancarella, "Virtual inertia response and frequency control ancillary services from hydrogen electrolyzers," *IEEE Trans. Power Syst.*, vol. 38, no. 3, pp. 2447–2459, May 2023.

[51] Y. Song, S. Sahoo, Y. Yang, and F. Blaabjerg, "Stability constraints on reliability-oriented control of AC microgrids–Theoretical margin and solutions," *IEEE Trans. Power Electron.*, vol. 38, no. 8, pp. 9459–9468, Aug. 2023.

[52] F. Garcia-Torres, C. Bordons, J. Tobajas, J. J. Marquez, J. Garrido-Zafra, and A. Moreno-Munoz, "Optimal schedule for networked microgrids under deregulated power market environment using model predictive control," *IEEE Trans. Smart Grid*, vol. 12, no. 1, pp. 182–191, Jan. 2021.

[53] P. García, J. P. Torreglosa, L. M. Fernández, F. Jurado, R. Langella, and A. Testa, "Energy management system based on techno-economic optimization for microgrids," *Electric Power Syst. Res.*, vol. 131, pp. 49–59, 2016.

[54] A. M. Alonso, G. Matute, J. Yusta, and T. Coosemans, "Multi-state optimal power dispatch model for power-to-power systems in off-grid hybrid energy systems: A case study in Spain," *Int. J. Hydrogen Energy*, vol. 52, pp. 1045–1061, 2023.

[55] Y. Zheng, S. You, H. W. Bindner, and M. Münster, "Optimal day-ahead dispatch of an alkaline electrolyser system concerning thermal–electric properties and state-transitional dynamics," *Appl. Energy*, vol. 307, 2022, Art. no. 118091.

[56] M. B. Abdelghany, V. Mariani, D. Liuzza, O. R. Natale, and L. Glielmo, "A unified control platform and architecture for the integration of wind-hydrogen systems into the grid," *IEEE Trans. Automat. Sci. Eng.*, early access, Jul. 12, 2023, doi: 10.1109/TASE.2023.3292029.

Ahmed Al-Durra (Senior Member, IEEE) received the B.Sc., M.Sc., and Ph.D. degrees in electrical and computer engineering from Ohio State University, Columbus, OH, USA, in 2005, 2007, and 2010, respectively.
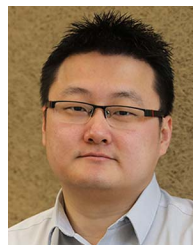
He is currently a Professor with the Electrical Engineering and Computer Science Department, Khalifa University, Abu Dhabi, UAE. He is also the Associate Provost for Research with Khalifa University. He has authored or co-authored more than 340 scientific articles in top-tier journals and refereed international conference proceedings. His research interests are applications of control and estimation theory on power systems stability, micro and smart grids, renewable energy systems and integration, and process control.

Dr. Al-Durra has supervised/co-supervised more than 30 Ph.D./Master's students. He is leading the Energy Systems Control and Optimization Lab under the Advanced Power and Energy Center, an Editor of IEEE TRANSACTIONS ON SUSTAINABLE ENERGY AND IEEE POWER ENGINEERING LETTERS, and an Associate Editor for the IEEE TRANSACTIONS ON INDUSTRY APPLICATIONS.

Hatem H. Zeineldin (Senior Member, IEEE) received the B.Sc. and M.Sc. degrees in electrical engineering from Cairo University, Giza, Egypt, in 1999 and 2002, respectively, and the Ph.D. degree in electrical and computer engineering from the University of Waterloo, Waterloo, ON, Canada, in 2006.

He was with Smith and Andersen Electrical Engineering, Inc., North York, ON, USA, where he was involved in projects, including distribution system designs, protection, and distributed generation. He was a Visiting Professor with the Massachusetts Institute of Technology, Cambridge, MA, USA. He is currently with the Khalifa University of Science and Technology, Abu Dhabi, UAE, and on leave from the Faculty of Engineering, Cairo University. His current research interests include distribution system protection, distributed generation, and microgrids.

Muhammad Bakr Abdelghany (Member, IEEE) received the B.Sc. degree in computer and systems engineering and the M.Sc. degree in electrical engineering from the Faculty of Engineering, Minia University, Minya, Egypt, in 2010 and 2015, respectively, the Ph.D. degree in systems and control engineering from the University of Sannio, Benevento, Italy, in 2022.

In 2010, he served as a Teaching Assistant with the Department of Computer and Systems Engineering, Minia University, Egypt. He is currently with the KUST (Tenure-track Researcher) and on leave from the Faculty of Engineering (Assistant Professor), Minia University. His research interests include control synthesis, cyber-physical systems, computer-controlled systems, green hydrogen production, renewable energy systems, and embedded systems.

Dr. Abdelghany has supervised/co-supervised 10 Ph.D./Master's students. He is also the Guest Editor for a special issue under IEEE TRANSACTIONS ON INDUSTRY APPLICATION on control applications in Hydrogen Energy systems. He is a Reviewer for various reputed journals, including the control community (IEEE TRANSACTIONS ON AUTOMATIC CONTROL, IEEE TRANSACTIONS ON CONTROL SYSTEM TECHNOLOGY, IEEE CONTROL SYSTEMS LETTERS, AND IEEE TRANSACTIONS ON CONTROL OF NETWORK SYSTEMS), Power and Energy Society (IEEE TRANSACTIONS ON SUSTAINABLE ENERGY, IEEE TRANSACTIONS ON POWER SYSTEMS, APPLIED ENERGY, ENERGY, ENERGY CONVERSION AND MANAGEMENT, AND RENEWABLE AND SUSTAINABLE ENERGY REVIEWS), and Robotics and Automation Society (IEEE TRANSACTIONS ON AUTOMATION SCIENCE AND ENGINEERING, DRONES, AND IEEE TRANSACTIONS ON ROBOTICS). He was honored with prestigious academic awards as an outstanding Reviewer for IEEE TRANSACTIONS ON SUSTAINABLE ENERGY in 2023.

Fei Gao (Fellow, IEEE) received the Ph.D. degree in renewable energy from University of Technology of Belfort-Montbeliard (UTBM), France, in 2010.

He is currently a Full Professor with the School of Energy and Computer Science, UTBM.

Dr. Gao specializes in hydrogen fuel cells for transportation and digital twin technology in modern power electronics and energy systems. He is a Fellow of both IEEE and IET. He is the recipient of Distinguished Youth Doctor Award, 2020 "IEEE J. David Irwin Early Career Award" from the IEEE Industrial Electronics Society, 2022 "Leon-Nicolas Brillouin Award" from SEE France, and 2022 industrial "Sustainable Future Visionary Award" from Typhoon HIL. He currently serves as the Editor-in-Chief of IEEE Industrial Electronics Technology News (ITeN), the Deputy Editor-in-Chief of IEEE TRANSACTIONS ON TRANSPORTATION ELECTRIFICATION, and holds leadership roles in various IEEE societies, including the Chair of the Award Committee and of the Constitution & Bylaws Committee of the IEEE Transportation Electrification Council, the Vice-Chair of the Technical Committee on Electrified Transportation Systems of the IEEE Power Electronics Society and Vice-Chair of the Industrial Automation and Control Committee of the IEEE Industry Applications Society.